https://dx.doi.org/10.22161/ijaers.73.51 *ISSN: 2349-6495(P) | 2456-1908(O)*

Numerical Analysis of Free Convection flow in Square Enclosure Partially Heated from below using the Multigrid Method

Lara Maria Moreira[1], Maximilian Serguei Mesquita[2,*], Marcelo J.S. de Lemos[3,*]

[1]Graduate Student of Petroleum Engineering, Universidade Federal do Espírito Santo – UFES/CEUNES, 29932-540 São Mateus - ES, Brazil
[2]Departamento de Engenharias e Tecnologia – DETEC, Universidade Federal do Espírito Santo – UFES/CEUNES, 29932-540 São Mateus - ES, Brazil
Departamento de Energia – IEME, Instituto Tecnológico de Aeronáutica – ITA, 12.228-900 São José dos Campos, SP, Brasil
[*] Corresponding author

Abstract*— *The present work investigates the efficiency of the Multigrid method when applied to solve two-dimensional laminar steady free convection flow in a square enclosure partially heated from below. The numerical method includes finite volume discretization with upwind scheme on structure orthogonal regular meshes. The performance of the correction storage (CS) Multigrid algorithm is compared for different numbers of sweeps in each grid level. Up to two grids, for both Multigrid V- and W- cycles, are presented. The results are mainly analyzed in terms of the average heat transfer at the walls of the enclosure and Multigrid performance on the rate of convergence. It is also shown that convective heat transfer has a characteristic behavior for each boundary conditions adopted in given ranges of the governing parameters.

Keywords*— *Multigrid, Free convection, Finite Volume, Numerical Methods.

Abbreviated title: Numerical Analysis of Free Convection Using the Multigrid Method

Nomenclature

C_p	Specific heat at constant pressure
CPU	CPU Time (s)
g	Gravitational acceleration
Gr	Grashof number
h	Average convective heat transfer coefficient
H	Height of the enclosure
L	Domain length / height
k	Thermal conductivity of the fluid
M	Maximum grid number
Nu	Average Nusselt number,
p	Thermodynamic pressure
Pe	Peclet number
Pr	Prandtl number
R_{ij}	Residue
T	Temperature
t_w	Temperature of the isothermal vertical wall

https://dx.doi.org/10.22161/ijaers.73.50 *ISSN: 2349-6495(P) | 2456-1908(O)*

S_φ	Source term for φ, $\varphi = U, V, p, t$
U	Component of velocity along x axis
V	Component of velocity along y axis
w	Width of the inlet, and the vent
x, y	Cartesian coordinates

Subscrit

i, j	Nodal index
in	Input values
k	Grid level
nb	Neighboring

Greeks Characters

α	Thermal diffusivity, $\rho C_p / k$
β	Coefficient of thermal expansion, $\left(\frac{-1}{\rho}\right)\left(\frac{\partial p}{\partial t}\right)_p$
ε	Dimensionless length of the heat source, $= l/L$
ν	Kinetic viscosity of the fluid
μ	Dynamic viscosity
ρ	Density of fluid
φ	General variable
Γ_φ	Diffusion coefficient for φ, $\varphi = U, V, p, t$
ν^{cg}	Number of Coarsest-grid iterations
ν^{pre}	Number of pre–smoothing iterations
ν^{post}	Number of post–smoothing iteration

I. INTRODUCTION

This study promotes a discussion surrounding the efficiency of the Multigrid method applied in a specific configuration. Multigrid methods have been used in many different calculations as a result of its facilitated converge capability.In single-grids, convergence rates solutions are greater in the beginning of calculations, reducing this sensibility while the iterative processes goes on. This hard-to-converge behavioris due to the iterative methods which smooth out only those Fourier error components of wavelengths smaller than or equal to the grid size. Naturally, this effect becomes more significant as the mesh becomes refined. At another level, Multigrid methods cover a broader range of wavelengths trough relaxation on more than one grid, making it easier to converge.

A Multigrid cycle is a repetitive procedure practiced at each grid level according to the grid hierarchy. The V- and W- cycles are types of Multigrid that determines the convergence criterion and the number of iterations in each step along consecutive grid levels visited by the algorithm. Within each cycle, the intermediate solution is relaxed before (pre-) and after (post-smoothing) the transportation of values to coarser (restriction) or to finer (prolongation) grids [[1]-[3]].

The Multigrid method can be roughly classified into two major categories. The CS formulation, where algebraic equations are solver for the corrections of the variables and the Full Approximation Storage (FAS) scheme, where variables themselves are handled in all grid levels. Since much work has been done on both major classifications, specific recommendations are admitted. The application of

https://dx.doi.org/10.22161/ijaers.73.50 *ISSN: 2349-6495(P) | 2456-1908(O)*

the CS formulation is recommended for the solution of linear problems being the FAS formulation more suitable to non-linear cases [[1]-[3]].Therefore, an exception has been disclosed in the work of [[4]], who reported predictions for the Navier-Stokes equations successfully applying the Multigrid CS formulation. In the literature, however, not too many attempts in solving non-linear problems with Multigrid linear operators are found.

Acknowledging the advantages of using multiple grids, [[5]] presented numerical computations applying this technique to recirculating flows in several geometries of engineering interest. There, the correction storage (CS) formulation was applied to non-linear problems. Later [[6]], analyzed the effect of Peclet number and the use of different solution cycles when solving the temperature field within flows with a given velocity distribution. In all those cases, the advantages in using more than one grid in iterative solution was confirmed, furthermore, [[7]], introduced the solution of the energy equation in their Multigrid algorithm. Temperature distribution was calculated solving the whole equation set together with the flow field as well as uncoupling the momentum and energy equations. A study on optimal relaxation parameters was there reported. More recently, [[8]] analyzed the influence of the increase of points of the mesh and optimal values of the parameters of the Multigrid cycle for different geometries. Also, [[8]-[11]], presented a study on optimal convergence characteristics in solution of conductive-convective problems.

Much work has been done with enclosure geometries, studying heat and mass transfer, (simultaneously or not) because of its engineering response value. The reason for the attention behind the physical nature of buoyance-induced flows is well represented in [[12]]. Cooling of electronic devices before its excessive heating, recovery of remnant oil in petroleum reservoirs, dispersion of atmospheric pollution and its implications in adjacent cities,spreading chemical and nuclear waste in soil, are just some examples of its importance.

The current work considers that free convection conditions can be imposed inside a square cavity and aims to study the interactions between buoyancy forces and heat elements inside. This application involves the work showed in the literature that has been discussed by many authors. The interaction between buoyancy forces and the heated elements and the numerical analysis of Multigrid solution applied into momentum and heat transfer forms the main objective of current work.

II. GOVERNING EQUATIONS

The following equations emerge from the mathematical descriptions of fluid flow and convective heat transfer in the enclosure. These governing equations are based on two-dimensional, incompressible, laminar flow in Cartesian coordinate system.

$$\frac{\partial U}{\partial x}+\frac{\partial V}{\partial y}=0 \tag{1}$$

$$U\frac{\partial U}{\partial x}+V\frac{\partial V}{\partial y}=-\frac{1}{\rho}\frac{\partial p}{\partial x}+\nu\nabla^2 U \tag{2}$$

$$U\frac{\partial V}{\partial x}+V\frac{\partial V}{\partial y}=-\frac{1}{\rho}\frac{\partial p}{\partial y}+\nu\nabla^2 V+g\left[\beta_T\left(T-T_{ref}\right)\right] \tag{3}$$

$$U\frac{\partial T}{\partial x}+V\frac{\partial T}{\partial y}=\alpha\nabla^2 T \tag{4}$$

Where U and V are the velocity components in x and y directions respectively, ρ is the density of the fluid, p is the total pressure and ν is the kinematic viscosity of the fluid. The gravity acceleration is defined by g and β_T is the thermal expansion coefficient. T and T_{ref} are the temperature and the reference temperature, respectively, and α is the thermal diffusivity.

The transport dimensionless parameters, Grashoff (Gr), which provides the relationship between fluid buoyancy and viscosity, Prandtl (Pr), that provides the relationship of momentum diffusivity and thermal diffusivity and the Rayleigh number (Ra), which is an associated number of buoyancy-driven flow (natural convection) are given by:

$$Gr=\frac{g\beta_T\Delta T H^3}{\nu^2},\ \mathrm{Pr}=\frac{\nu}{\alpha} \tag{5}$$

$$Ra=Gr\cdot\mathrm{Pr} \tag{6}$$

III. NUMERICAL MODEL

The solution domain consist on a number of rectangular control volumes (CV), resulting in a structure orthogonal non-uniform mesh. Grid points are located according to a

https://dx.doi.org/10.22161/ijaers.73.50 *ISSN: 2349-6495(P) | 2456-1908(O)*

cell-centered scheme and velocities are store in a collocated arrangement[[13]]. A typical CV with its main dimensions and internodal distances is sketched in Fig. **Error! Reference source not found.**.

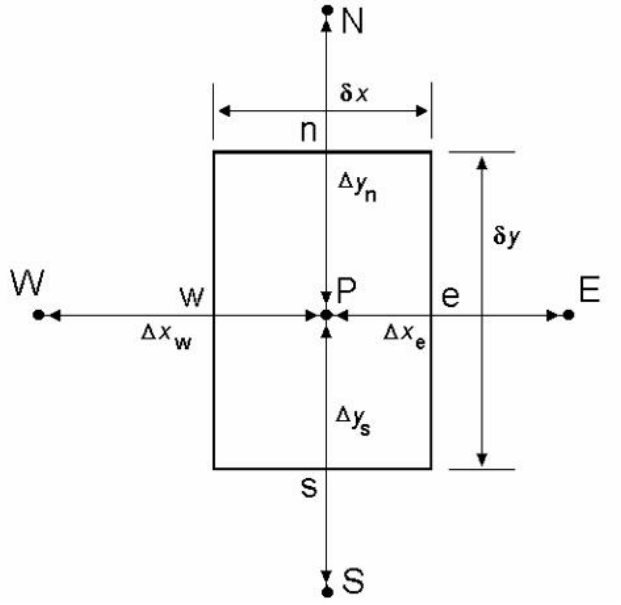

Fig. 1– Control Volume for discretization.

Writing equations (1), (2), (3) and (4) in terms of a general variable $\varphi = \{1, U, V, T\}$ with $\Gamma_\varphi = \left\{0, \mu, \mu, \mu/\mathrm{Pr}\right\}$ and $S_\varphi = \left\{0, -\frac{\partial P}{\partial x}, -\frac{\partial P}{\partial y}, 0\right\}$ one gets,

$$\frac{\partial}{\partial x}\left(\rho U\varphi - \Gamma_\varphi \frac{\partial \varphi}{\partial x}\right) + \frac{\partial}{\partial y}\left(\rho V\varphi - \Gamma_\varphi \frac{\partial \varphi}{\partial y}\right) = S_\varphi \quad (7)$$

After integrating it over the CV of Fig.**Error! Reference source not found.**,

$$\int_{\delta V}\left[\frac{\partial}{\partial x}(\rho U\varphi) + \frac{\partial}{\partial y}(\rho V\varphi)\right]dV = \int_{\delta V}\left[\frac{\partial}{\partial x}\left(\Gamma_\varphi \frac{\partial \varphi}{\partial x}\right) + \frac{\partial}{\partial y}\left(\Gamma_\varphi \frac{\partial \varphi}{\partial y}\right)\right]dV + \int_{\delta V} S_\varphi dV \quad (8)$$

A set of algebraic equations are resulted from the integration of terms in (8), as one can name it, convection, diffusion, and source. Since these procedures are described somewhere else (e.g. **Error! Reference source not found.**) they are not repeated in this paper. To summarize, convective terms are discretized using the upwind differencing scheme (UDS) and diffusive fluxes make use of the central differencing scheme (CDS).

The final discretization for grid node P is done by using the integrated transport equation (8) with the substitution of all approximate expressions for interface values and gradients.

$$a_P\varphi_P = a_E\varphi_E + a_W\varphi_W + a_N\varphi_N + a_S\varphi_S + b \quad (9)$$

With the east face coefficient, for example, being defined as:

$$a_E = \max\left[-C_e, 0\right] + D_e \quad (10)$$

In (10), $D_e = \mu_e \delta_y / \Delta x_e$ and $C_e = (\rho U)_e \delta_y$ are the diffusive and convective fluxes at the CV east face, respectively, and, as usual, the operator $\max[a,b]$ returns the greater between a and b.

IV. MULTIGRID TECHNIQUE

The wanted effect of the Multigrid approach in this work is for the convergence rate to become independent on

https://dx.doi.org/10.22161/ijaers.73.50 *ISSN: 2349-6495(P) | 2456-1908(O)*

the grid spacing and the numerical solution faster. The task behind the Multigrid method is to involve a hierarchy of successively coarsened grids into the iterative solution process. When done, an adequate strategy for the movement through the different grid levels should follow, along with consistently transferring data with the discretization scheme between the grids. This process allows an efficient error reduction over a wide spectrum of frequencies.

If an iterative scheme as the one described below is applied to the system of equations on a given grid, it turns out only those frequencies of the solution error can be reduced efficiently, which corresponds to the grid spacing. The high frequencies of the error are reduced a few iterations, while the low frequencies nearly remain unchanged. At another level, the steps usually taken in Multigrid algorithm are the reduction of high frequency errors(smoothing), computation of residual error(residual computation), decimation of the residual error to a coarser grid(restriction), and the interpolation into a finer grid. The present development about the Multigrid technique is also presented in [[5],[6],[10],[11]] and for this reason the development is not repeated here.

V. RESULTS AND DISCUSSION

The computer code was run on an IBM PC machine with an INTEL CORE 2 DUO 2.0 GHz processor. Grid independence studies were conducted such that the solutions presented herein are essentially grid independent. For both cycles, pre- and post-smoothing iterations were accomplished via the Gauss-Seidel algorithm while, at the coarsest-grid, the TDMA method has been applied [[13]].

The Fig. 2 a) represent general geometries that were run with the finest grid having $66x66$ grid points highlighted in Fig. 2 b).

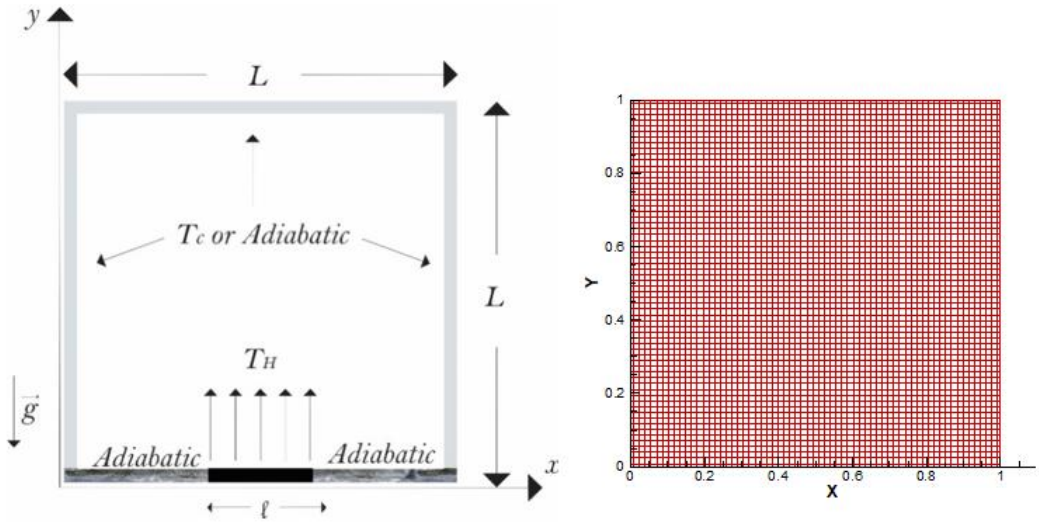

Fig. 2 - a) Geometries and boundary conditions and b) computational grid.

The main difference between the present work and the work from [[14]] is that here it is used the prescribed values (temperature - T_H) while in the reference work is used heat fluxes. This particularity reinforces a permanent regime with constant physical properties of the flux.

In order to understand better the implications of this new configuration and construct a simpler idea of the square cavity, for comparison meaning,Fig. 3 shows the streamlines and isotherms, respectively, of a clear square cavity heated on the left and cooled from the opposing side for Rayleigh numbers ranging from 1×10^3 to 1×10^6.

https://dx.doi.org/10.22161/ijaers.73.50 *ISSN: 2349-6495(P) | 2456-1908(O)*

Steam Functions Temperature

$Ra = 1 * 10^3$

a) b)

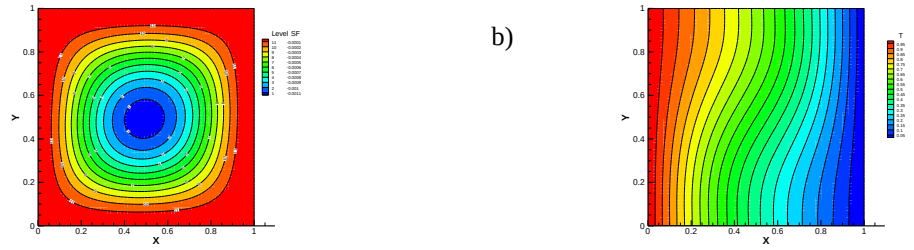

$Ra = 1 * 10^4$

c) d)

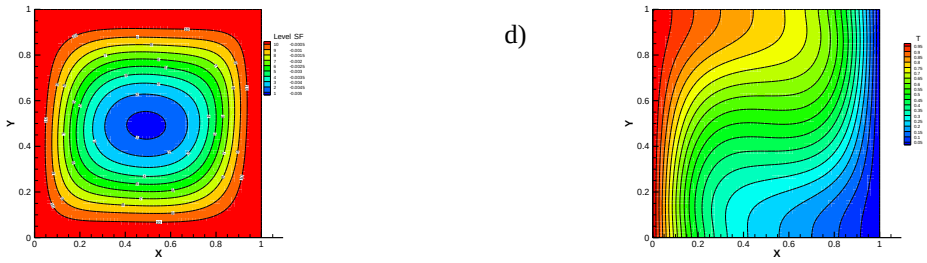

$Ra = 1 * 10^5$

e) f)

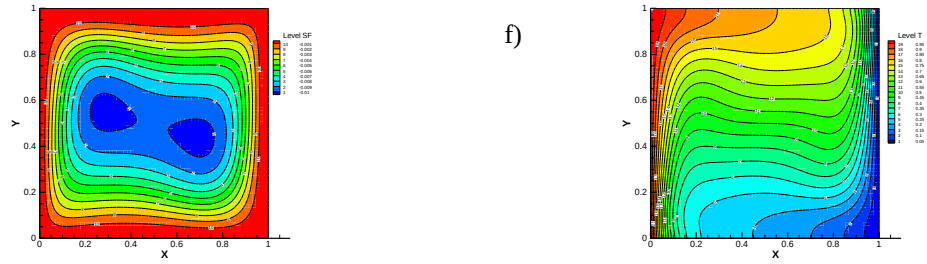

$Ra = 1 * 10^6$

g) h)

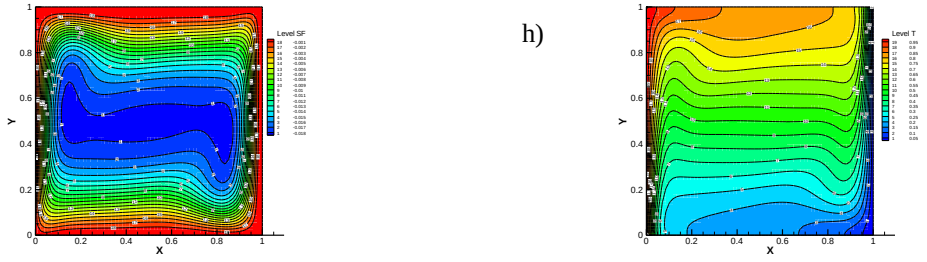

Fig. 3 - Natural Convection in Square Cavity from left to bottom $Ra = 1 * 10^3$, $Ra = 1 * 10^4$, $Ra = 1 * 10^5$ *and* $Ra = 1 * 10^6$, *respectively.*

In Fig. (3a), $Ra = 1 \times 10^3$, the streamlines indicates an existence ofone centered vortex while corresponding isotherms, Fig. (3b), indicates a conductive heat transfer, expressed by the almost parallel pattern with the heated wall. The vortex is generated by the horizontal temperature gradient across the section. This gradient, $\frac{\partial T}{\partial y}$ is negative everywhere, inducing a clockwise oriented vorticity.

When the Rayleigh number is increased to $Ra = 1 \times 10^4$, Fig. (3c), the vortex in the middle of the

https://dx.doi.org/10.22161/ijaers.73.50 *ISSN: 2349-6495(P) | 2456-1908(O)*

cavity starts to shape differently, slightly into a more elliptic configuration. The isotherms, Fig (3d), therefore, have a considerable convection advance, and the parallel configuration is undone, especially in the middle of the cavity.Temperature gradients are stronger near the vertical walls, but decrease in the center region.

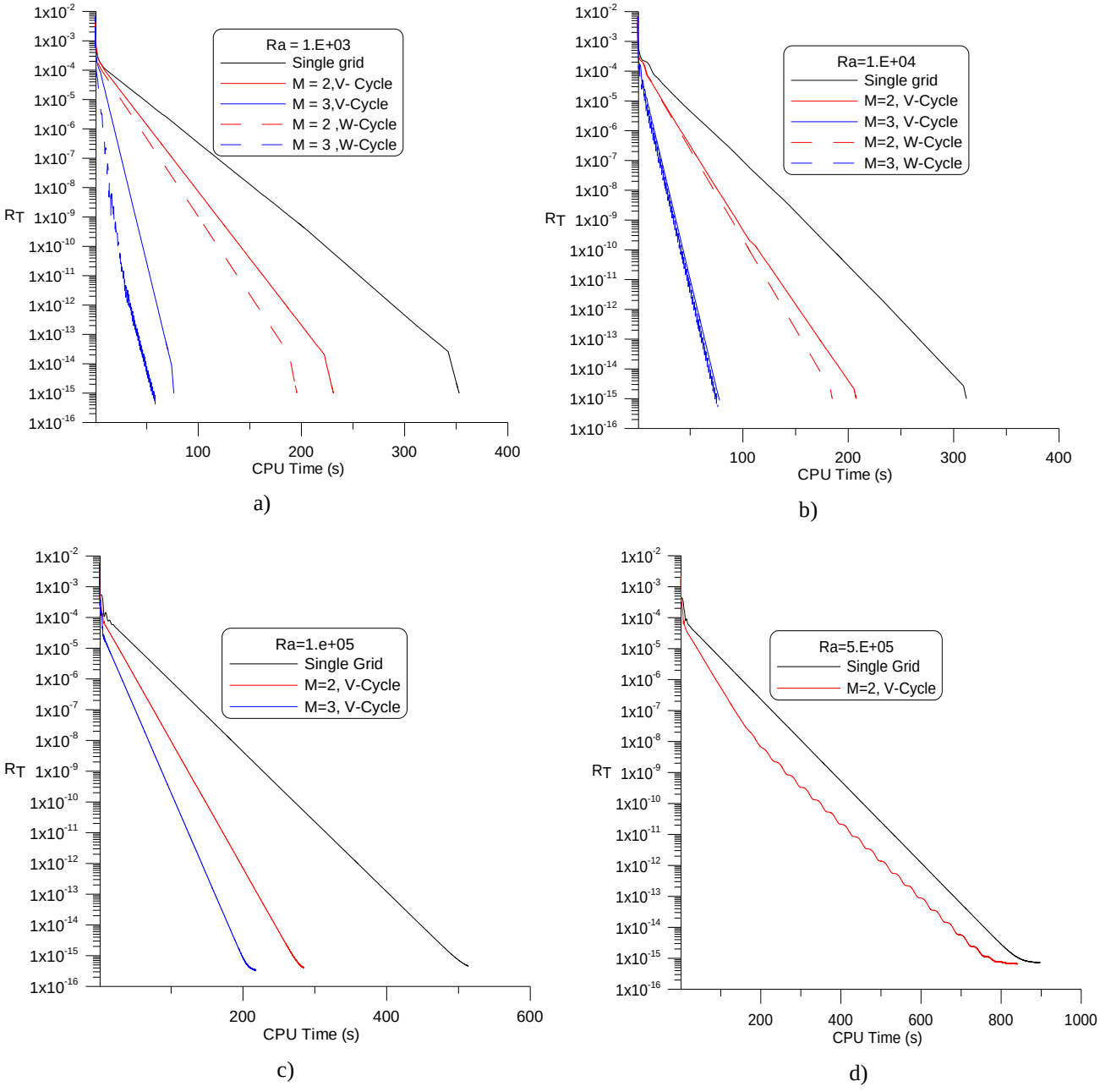

Fig. 4 – Temperatures residues history for different values of the Rayleigh number: a) $Ra = 1 * 10^3$, *b)* $Ra = 1 * 10^4$, *c)* $Ra = 1 * 10^5$ *and d)* $Ra = 1 * 10^5$

https://dx.doi.org/10.22161/ijaers.73.51 *ISSN: 2349-6495(P) | 2456-1908(O)*

For $Ra = 1\times10^5$, Fig. (3e), the elliptical behavior continuous and the centered vortex is stretched so that two secondary vortices can be shown inside of it. Heat transfer by convection in the viscous boundary layer alters the temperature distribution to such an extent that temperature gradients in the center of the domain are close to zero. Fig. (3e) shows that, with this change in the sign of the source term negative, vorticity is induced within the domain. This also causes the development of secondary vortices in the core. Fig. (3f) continuous its convection advance in the square cavity indicating a faster movement of the flux closer to the walls.

Finally, in Fig. (3g), $Ra = 1\times10^6$, one can see an initiative attempt for a three vortices configuration inside the main vortex. Corresponding Fig. (3h) shows that heat transfer is mostly convective, again due to the faster movement on boarders.

Fig.4 above, shows the residue history for temperature with different values of $Ra = 1\times10^3$ to 5×10^5, up to 3 grids, for the V- and W-cycles. For a three grids, with $Ra = 1\times10^3$ one can notice a slight advantage in using the W-cycle, while in $Ra = 1\times10^4$ that advantage is almost unnoticeable. Now, looking at higher Rayleigh numbers, $Ra = 1\times10^5$ to $Ra = 5\times10^5$, the V-cycle can be better stipulated. This change of cycle due to the increase in the Rayleigh number happens because of the changing flux attempt to turn turbulent. An explanation for this matter are on many references of Multigrid approximation on turbulent flow, which in most of the cases use the FAS formulation.

Another configuration, shows the results of isotherms and streamlines of a clear square cavity heated on the bottom and cooled from the top for a Rayleigh number of $Ra = 4\times10^4$. The work of [[12]] is used for comparison.

Reference [[12]]

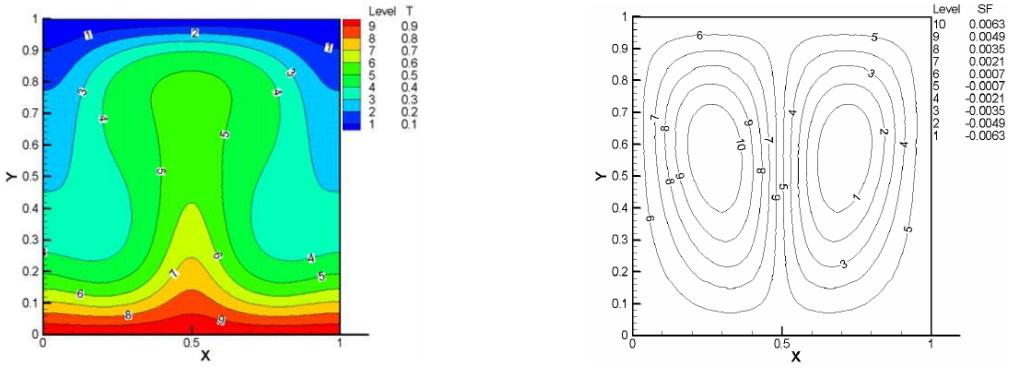

Present Results

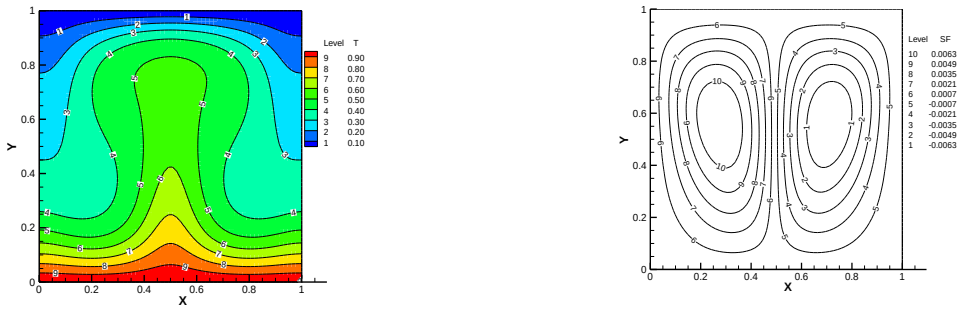

Fig. 5 – Isotherms and Streamlines for a clear square cavity heated from bottom and from the ceiling for $Ra = 1 * 10^4$*, comparison between [[12]] and present research.*

In Fig. 5, it is easy to see the similarities in the results of bothworks. Studying these results, one can note the plume shaped structure starting at the bottom of the cavity moving towards the top. Circulatory motion brings the bottom hot

https://dx.doi.org/10.22161/ijaers.73.50 *ISSN: 2349-6495(P) | 2456-1908(O)*

temperature stream up to the top wall, substantially penetrating into the flow core.

From these results, is expected a better understanding and a certain familiarization with the final configuration, Fig. 2a, due to the heated bottom in the square cavity. Additionally,Fig. 5 representsthe only possible solutions for that Ra number, reinforcing the final results and the geometry qualitatively.

Final configuration, square cavity partially heated from above, is separated into two different forms, denoted as C_1 and C_2. The C_1 structure hasboth lateral walls cooled at temperature T_c and top wall adiabatic, while C_2 hasleft lateral wall and top wall cooled at temperature T_c and right lateral wall adiabatic. Fig. 6 is a representative scheme of C_1 and C_2. Notice that for allconfigurations the total surfaces of the cooled walls are identical.

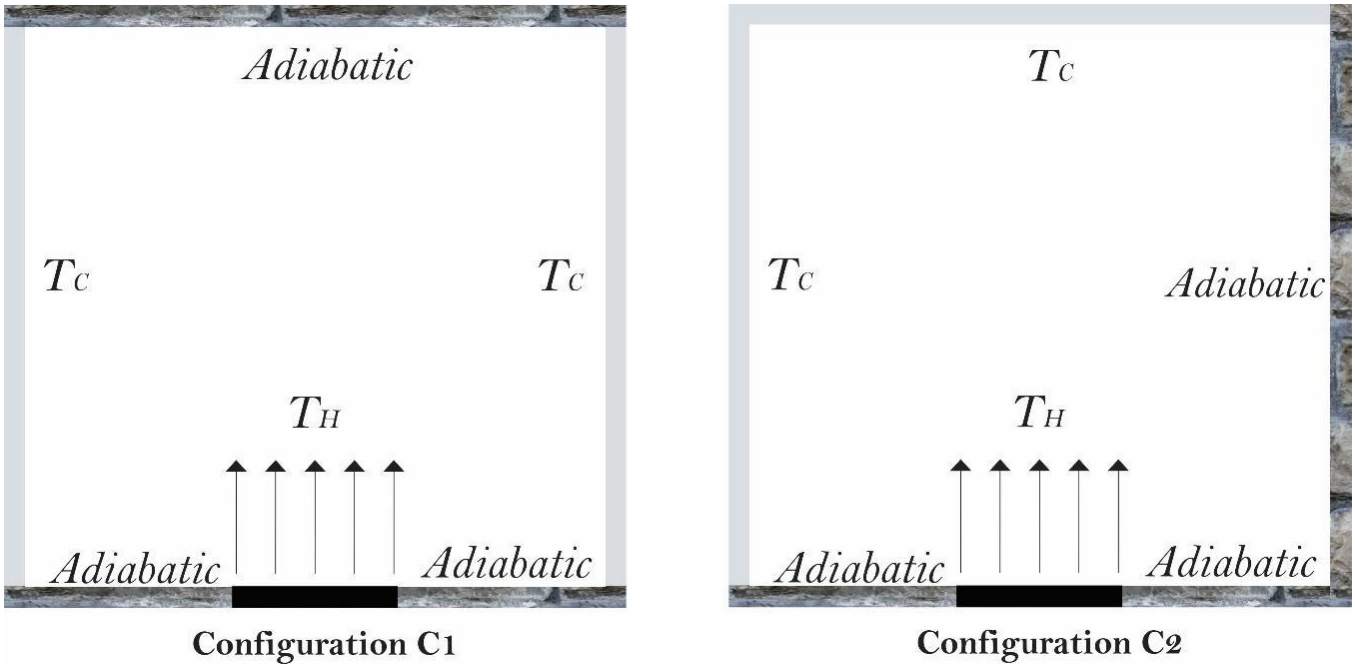

Fig. 6 - Thermal configurations of the cavity.

https://dx.doi.org/10.22161/ijaers.73.50 *ISSN: 2349-6495(P) | 2456-1908(O)*

$Ra = 4\times10^4$

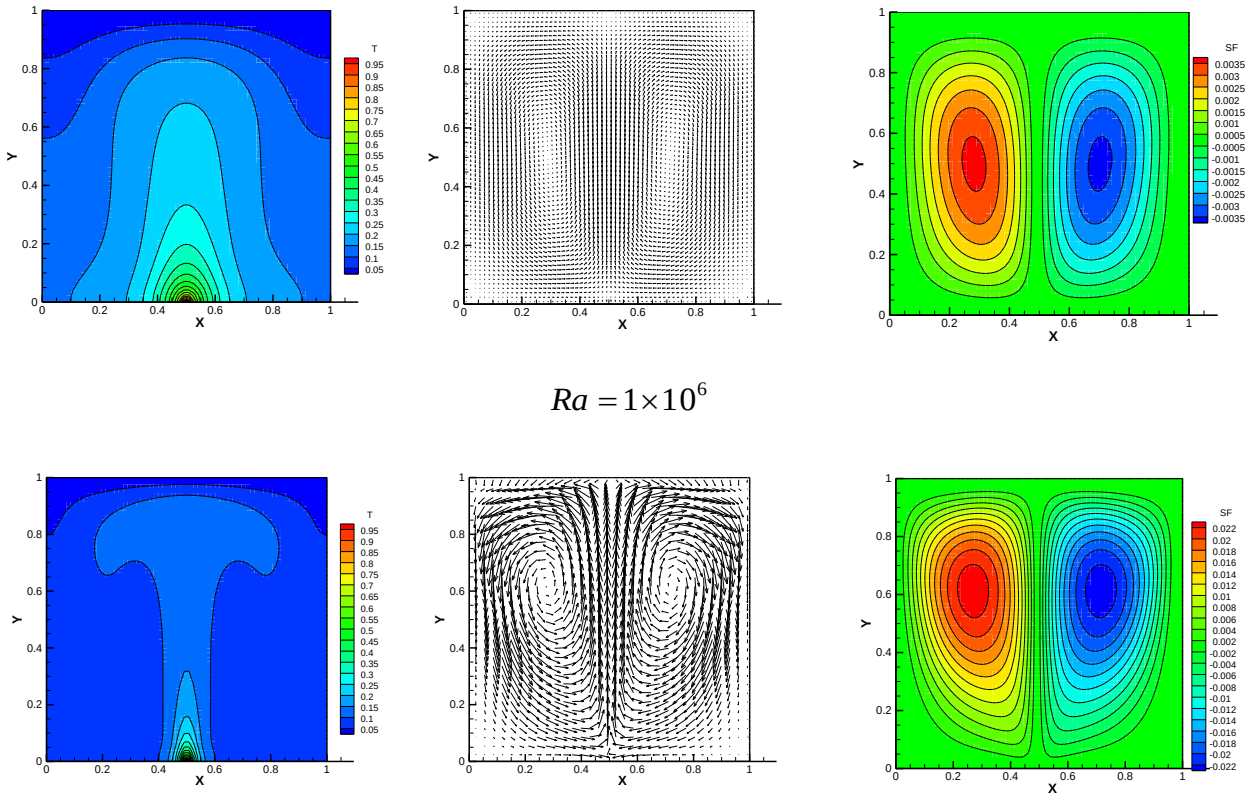

$Ra = 1\times10^6$

Fig. 7 – Isotherms, vectors and isotherms in the cavity for $\varepsilon = 0.03$.

Final results can be seen in Fig. 7, 8 and 9 for C_1 and C_2 conditions, side by side, as Rayleigh number increases top to bottom. As ε was incremented, the streamlines and isotherms related are plotted.

First observation lies on the boundary thermal conditions. When these conditions are symmetrical, about the vertical mid plane, i.e., case C_1, the fluid motion is also symmetrical and two counter-rotating cells are formed in the cavity. The isotherms are also symmetrical about the vertical mid plane and it is noticed that the temperature gradient becomes steeper and bigger at the hot surface where a thermal plume may be located.In case C_2, fluid flow takes a direction towards the adiabatic wall on the side of the cavity, making the flow asymmetric and characterized with a single-cell of anticlockwise circulation.

In each case the stagnation point is observed at the middle of the bottom wall. It is easy to see the similarity between case C_1 and the bottom-heated arrangement in Fig. 5, making a plume shaped pattern. Similar behaviors of the flow and thermal fields are observed at other Rayleigh numbers as an increment for the following Figures. Finally, Fig. 10 presents temperatures residues history for different values of the Rayleigh number, $Ra = 4\times10^4$ and $Ra = 1\times10^6$ for the case it was presented in Fig. 7. Once more again the Multigrid solution has the best results at least in the computational effort reduction.

https://dx.doi.org/10.22161/ijaers.73.50 *ISSN: 2349-6495(P) | 2456-1908(O)*

Boundary Condition - C_1 Boundary Condition - C_2

$Ra = 1\times10^4$

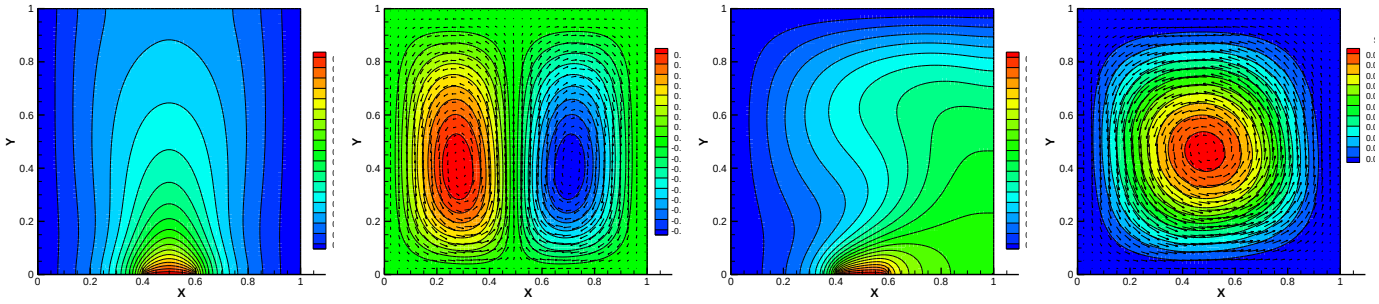

$Ra = 1\times10^5$

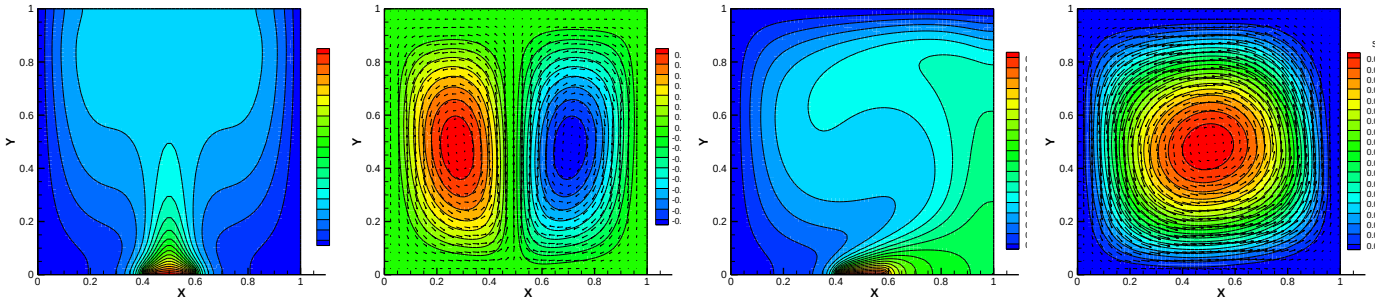

$Ra = 1\times10^6$

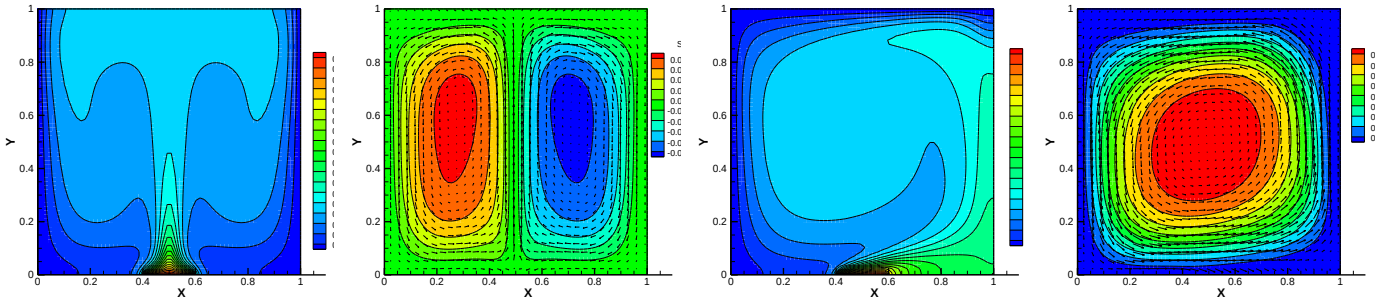

Fig. 8 - Streamlines and isotherms in the cavity for $\varepsilon = 0.2$.

https://dx.doi.org/10.22161/ijaers.73.50 *ISSN: 2349-6495(P) | 2456-1908(O)*

Boundary Condition - C_1 Boundary Condition - C_2

$Ra = 1\times10^4$

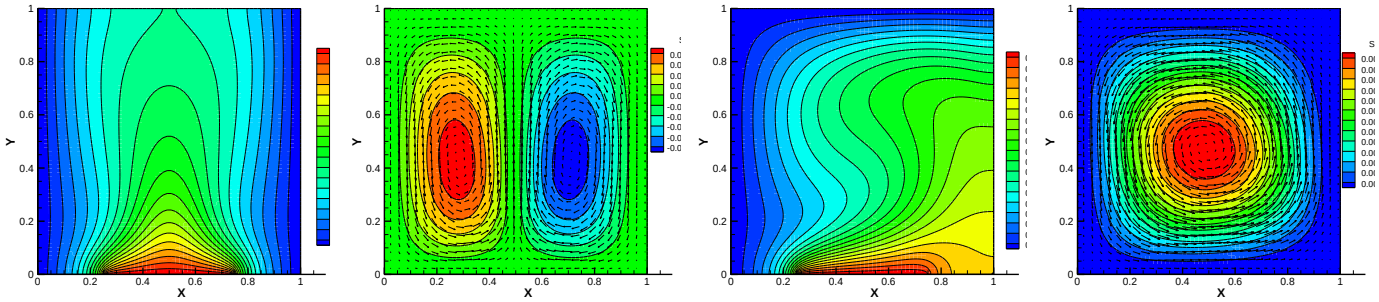

$Ra = 1\times10^5$

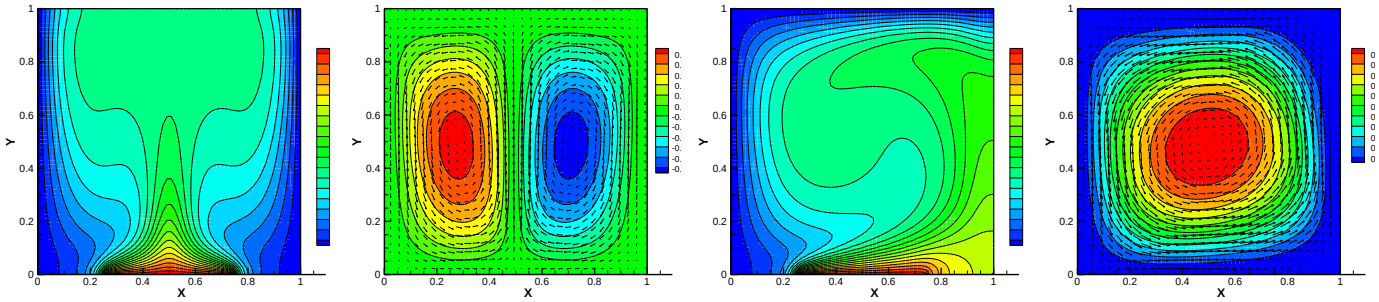

$Ra = 1\times10^6$

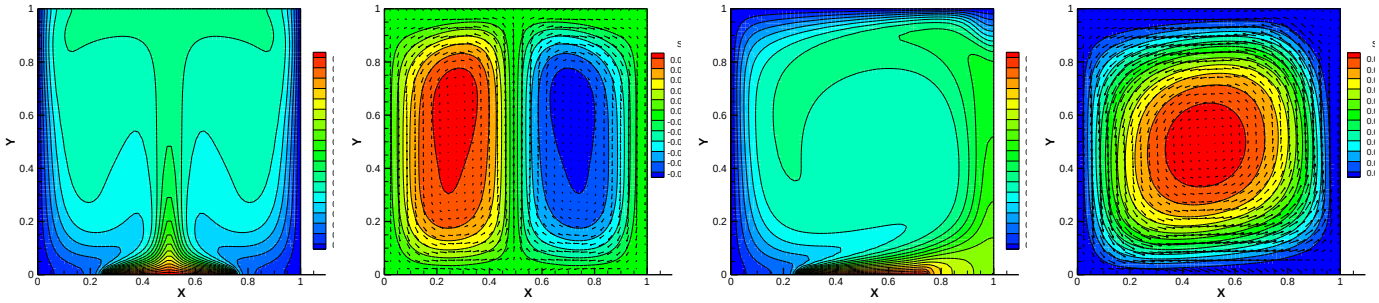

Fig. 9- Streamlines and isotherms in the cavity for $\varepsilon = 0.5$.

https://dx.doi.org/10.22161/ijaers.73.50 *ISSN: 2349-6495(P) | 2456-1908(O)*

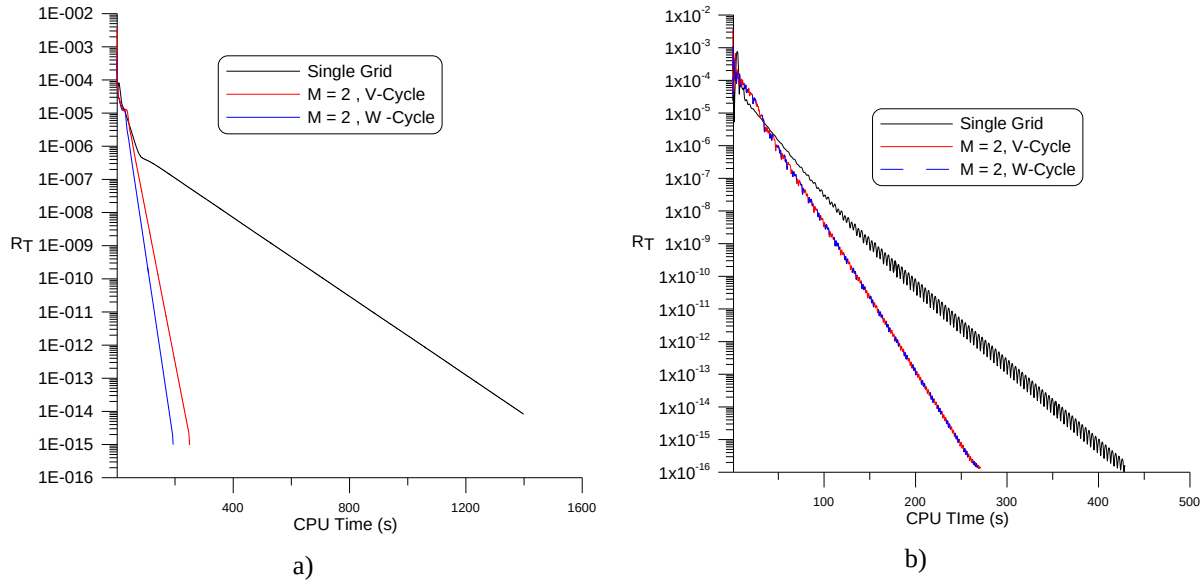

Fig. 10 – Temperatures residues history for different values of the Rayleigh number: a) $Ra = 1 * 10^4$ *and b)* $Ra = 1 * 10^6$

ACKNOWLEDGEMENTS

The authors are thankful to CAPES and FAPES, for their financial support during of this work.

REFERENCES

[1] Brandt., A1977, Multi-Level Adaptive Solutions to Boundary-Value Problems, Math. Comp., Vol. 31, No. 138, Pp. 333-390.

[2] Hackbusch, W., 1985, Multigrid Methods And Applications, Springer-Verlag, Berlin.

[3] Stüben, K., Trottenberg, U., 1982, Multigrid Methods, In Lect. Notes Math., Vol. 960, Pp. 1-76, Berlin

[4] Jiang, Y., Chen, C.P., Tucker, P.K., 1991, Multigrid Solutions of Unsteady Navier-Stokes Equations Using a Pressure Method, Num. Heat Transfer - Part A, Vol. 20, Pp. 81-93.

[5] Rabi, J.A., de Lemos, M.J.S., 2001, Optimization of Convergence Acceleration in Multigrid Numerical Solutions of Conductive-Convective Problems, Applied Mathematics and Computation, vol. 124, pp. 215-226.

[6] Rabi, J.A., de Lemos, M.J.S., 2003, Multigrid Correction-Storage Formulation Applied to the Numerical Solution of Incompressible Laminar Recirculating Flows, Applied Mathematical Modelling, v.27, n.9, p.717 - 732.

[7] De Lemos, M.J.S., Mesquita, M.S., 1999, Multigrid Numerical Solutions Of Non-Isothermal Laminar Recirculating Flows, Applications of Computational Heat Transfer, ASME-HTD-Vol. 364-3, ISSN: 0272-5673, ISBN: 0-7918-1656-7, Ed..L.C. White, Pg. 323-330.

[8] Mesquita, M.S., de Lemos, M.J.S., 2000a, Numerical Solution of Non-Isothermal Laminar Recirculating Flows Using The Multigrid Method, ENCIT 2000, Porto Alegre, RS, Brazil, 2000.

[9] Mesquita, M.S., de Lemos, M.J.S, 2004, Optimal Multigrid Solutions Of Two Dimensional Convection-Conduction Problems, Applied Mathematics and Computation, v. 152, n. 3, p.725-742.

[10] Mesquita, M. S.; Lemos, Marcelo Jose Santos de, 2005, Effect of Medium Properties on Convergence Rates of Multigrid Solutions of Laminar Flows in Permeable Structures. International Journal of Dynamics of Fluids Ijdf, Delhi - India, V. 1, N. 1.

[11] Mesquita, M.S., de Lemos, M.J.S, 2007, Mixed Convection In Square Vented Enclosure Filled With A Porous Material Using The Multigrid Method, AIChE Annual Meeting, Conference Proceedings.

[12] Braga, E. J., Turbulent Natural Convection in Porous Enclosures, Phd Thesis, ITA, 2003.

[13] Patankar, S.V., 1980, Numerical Heat Transfer And Fluid Flow, Mc-Graw Hill.

[14] Cheikh, N. B., Brahim, B. B.,Lili, T., Influence of thermal boundary conditions on natural convectionin a square enclosure partially heated from below, IJHMT, 34 (2007) 369–379.